

## GEOMETRY AND TOPOLOGY OF FINITE-GAP VORTEX FILAMENTS

THOMAS A. IVEY

*College of Charleston, Charleston, South Carolina 29424, USA*

**Abstract.** In this talk, I will discuss the vortex filament flow, and its connection with the nonlinear Schrödinger equation (NLS), the geometry of solutions to the filament flow that correspond to finite-gap solutions of NLS, and in particular, the relationship between geometric properties of the filament to features of the Floquet spectrum of a periodic NLS potential. These will be illustrated by the example of elastic rod centerlines. I will also discuss the geometric implications of symmetric Floquet spectra, and the topological implications of certain isoperiodic deformations of the spectrum that open up real double points.

### 1. The Vortex Filament Flow

The **vortex filament flow** is an evolution equation for space curves, given by

$$\frac{\partial \gamma}{\partial t} = \frac{\partial \gamma}{\partial x} \times \frac{\partial^2 \gamma}{\partial x^2} = \kappa \mathbf{B}, \quad \gamma \in \mathbb{R}^3 \quad (1)$$

where  $x$  is arclength,  $\kappa$  is Frenet curvature, and  $\mathbf{B}$  is the binormal. This was proposed in 1904 by da Rios (a student of Levi-Civita) as a model for self-induced motion of vortex lines in an incompressible fluid. An intuitive explanation of this model is that when a vortex line bends, the compression of streamlines inside the bend pushes the vortex line in a direction perpendicular to the osculating plane, with velocity proportional to the curvature. For example, circles translate with constant velocity (like a smoke ring). However, most planar initial curves immediately become non-planar under this flow.

#### 1.1. The Hasimoto Map

The vortex filament flow is regarded as completely integrable because of Hasimoto's discovery [6] that one can map solutions of (1) to solutions of the nonlinear

Schrödinger equation. If the curvature  $\kappa$  and torsion  $\tau$  of a solution of the vortex filament flow are packaged into a complex function of  $x$  and  $t$

$$q(x, t) = \frac{1}{2}\kappa e^{i\theta}, \quad \theta = \int \tau dx$$

then  $q$  satisfies the focusing cubic **nonlinear Schrödinger equation** (NLS)

$$iq_t + q_{xx} + 2q|q|^2 = 0. \quad (2)$$

For example, a translating circle of radius  $r$  corresponds to a “plane wave solution” of the NLS, given by

$$q = \frac{1}{2}\kappa e^{i\theta} = \frac{1}{2r} e^{it/(2r^2)}. \quad (3)$$

As it can be seen here, the time dependence of the antiderivative  $\theta$  in (3) is not arbitrary. In order to get (2), one must choose the antiderivative of torsion to satisfy

$$\theta_t = \frac{\kappa''}{\kappa} + \frac{1}{2}\kappa^2 - \tau^2.$$

This extra condition on  $\theta$  is compatible with  $\theta_x = \tau$ , because the torsion is a conserved density for the flow

$$\tau_t = \left( \frac{\kappa''}{\kappa} + \frac{1}{2}\kappa^2 - \tau^2 \right)_x.$$

Like the KdV, mKdV and sine-Gordon equations, the NLS is a completely integrable PDE. Why is this important? Because of the rich structure that such equations have.

## 1.2. Features of Completely Integrable PDE

Hasimoto’s discovery of the link between vortex filament flow and the NLS meant that filament flow can be regarded as a completely integrable PDE, in the same league as equations like KdV, mKdV and sine-Gordon. As a result, the filament flow enjoys the features common to “soliton” equations, such as:

- It is completely integrable as a Hamiltonian flow on the appropriate function space<sup>1</sup>, with an infinite sequence of conserved integrals

$$\int \tau dx, \quad \int \kappa^2 dx, \quad \int \kappa^2 \tau dx, \quad \int (\kappa')^2 + \kappa^2 \tau^2 - \frac{1}{4}\kappa^4 dx, \dots$$

and commuting flows

$$\begin{aligned} \gamma_{t_0} &= \mathbf{T}, & \gamma_{t_1} &= \kappa \mathbf{B}, & \gamma_{t_2} &= \frac{1}{2}\kappa^2 \mathbf{T} + \kappa' \mathbf{N} + \kappa \tau \mathbf{B} \\ \gamma_{t_3} &= \kappa^2 \tau \mathbf{T} + (2\kappa' \tau + \kappa \tau') \mathbf{N} + (\kappa \tau^2 - \kappa'' - \frac{1}{2}\kappa^3) \mathbf{B}, \dots \end{aligned}$$

<sup>1</sup>Usually, this is either the space of smooth closed curves of a fixed length, or balanced asymptotically linear curves [9].

(The ones given here were generated using recursion operators discovered by Langer and Perline [9].)

- It possesses explicit soliton and multi-soliton solutions, and an even larger class of explicit solutions known as **finite-gap solutions**.

Soliton solutions are, of course, often described as “solitary waves that move without changing shape or form”. The analogue for the filament flow would be a curve that moves by rigid motion. These curves turn out to be elastic rod centerlines.

### 1.3. Elastic Rod Centerlines

Kida [8] showed that the curves that move by rigid motion (i.e., a combination of rotation and translation in  $\mathbb{R}^3$ ) are Kirchhoff elastic rod centerlines. From a geometric point of view, these may be defined as curves that are critical for a Lagrangian of the form

$$\mathcal{F}[\gamma] = \lambda_1 \int dx + \lambda_2 \int \tau dx + \lambda_3 \int \frac{1}{2} \kappa^2 dx$$

with respect to variations that preserve the second derivatives of  $\gamma$  at the endpoints. (Again,  $x$  is arclength.) For  $\lambda_2 = 0$ , these are Eulerian elastic curves.

Langer and Singer [10] obtained expressions for the curvature, torsion, and position of the curve in terms of elliptic functions and elliptic integrals. They also showed that the Euler–Lagrange equations imply that the vector field

$$I = \lambda_2 \mathbf{T} + \lambda_3 \kappa \mathbf{B}$$

is the restriction to  $\gamma$  of a Killing field in  $\mathbb{R}^3$ . Therefore, elastic rod centerlines evolve by rigid motion (together with a constant-speed slide along the curve) under the  $\kappa \mathbf{B}$  flow.

Singer and the author [7] later showed that every torus knot type is realized by a one-parameter family of elastic rod centerlines. In fact, these centerlines fit into smooth families, which share a common rotational symmetry, and represent two complementary knot types, like the  $(2, 5)$  and  $(3, -5)$  knot types shown among the examples above. We call such a smooth family a *homotopy* of closed elastic rod centerlines.

These elastic rods are part of a larger class of vortex filament flow solutions that are derived from finite-gap solutions of the NLS. To understand how that works, we need to look at how to invert the Hasimoto map, i.e., producing a curve in  $\mathbb{R}^3$  from its Hasimoto potential  $q(x, t)$ .



Fig. 1. Models of the chains.

of the chains is assumed to be equal to the volume of the chain, and the volume of the chain is assumed to be equal to the volume of the chain.

$$\frac{V}{V_0} = \frac{V}{V_0} \quad (1)$$

$$V = \frac{V_0}{N} \quad (2)$$

where  $V$  is the volume of the chain,  $V_0$  is the volume of the chain,  $N$  is the number of chains, and  $V_0$  is the volume of the chain. The volume of the chain is assumed to be equal to the volume of the chain.

The volume of the chain is assumed to be equal to the volume of the chain. The volume of the chain is assumed to be equal to the volume of the chain.

One can check that  $\gamma$  is related to  $q$  via the Hasimoto map (3) if and only if (4) holds for a matrix solution  $\Psi$  of the linear system that is  $SU(2)$ -valued when  $\lambda$  is real.

Note that there are good reasons for evaluating (4) at a (real) value of  $\lambda$  other than zero. First, if we evaluate at a nonzero  $\Lambda_0 \in \mathbb{R}$ , then we get a different curve from (4), whose Frenet curvature is the same and whose torsion differs by an additive constant. But if we evaluate at  $\Lambda_0 \in \mathbb{R}$  but also modify  $q$  by a **gauge transformation**

$$\tilde{q}(x, t) = \exp(i(ax - a^2t))q(x - 2at, t), \quad a = -2\Lambda_0$$

then we get the same curve as we get from the Sym–Pohlmeyer formula using unmodified  $q$  and  $\lambda = 0$ .

### 3. Floquet Spectrum

One of our main interests is the topology (in particular, the knot type) of closed-loop solutions of the filament flow. If we are going to build such solutions using the inverse Hasimoto map, we must know how to obtain solutions that are smoothly closed.

First, for a closed curve, the potential  $q$  obtained by the Hasimoto map will not necessarily be periodic. Granted, the curvature and torsion will be periodic, but the antiderivative of torsion in (3) may not be periodic. However, we can perform a gauge transformation to obtain a periodic potential, that corresponds to the given curve via the Sym–Pohlmeyer formula, albeit evaluated at a nonzero value of  $\lambda$ .

Going in the other direction, suppose we start with a *periodic* solution of NLS, say, with  $q(x + L) = q(x)$ . (In this section we suppress dependence on time.) When does the Sym formula, evaluated at a suitable  $\lambda$ -value, give a closed curve of length  $L$ ? To answer this, we need to discuss the *Floquet spectrum* of the periodic potential  $q$ .

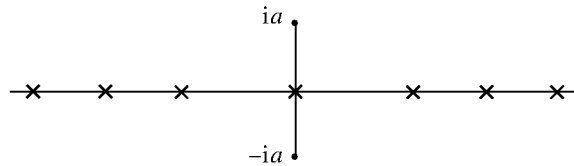
This spectrum is a subset of the complex plane made up of two kinds of  $\lambda$ -values. The *periodic spectrum* are the  $\lambda$ -values for which a non-trivial solution of the AKNS system is  $L$ -periodic (or antiperiodic) in  $x$ , while the *continuous spectrum* consists of  $\lambda$ -values for which the solutions are bounded as  $x \rightarrow \pm\infty$ . Both of these sets can be characterized in terms of the **Floquet discriminant**

$$\Delta(\lambda) = \text{trace} \left( \Psi(x + L)\Psi(x)^{-1} \right)$$

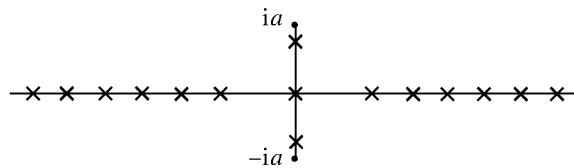
which is the trace of the linear system’s transfer matrix over one period  $L$ . Because the transfer matrix has determinant one, the solutions are periodic or antiperiodic exactly when the discriminant equals  $+2$  or  $-2$ , respectively. Points of the periodic spectrum consist of simple points or multiple points, etc., according to their multiplicity as zeros of  $\Delta(\lambda)^2 - 4$ .

### 3.1. Example: Spectrum of the Circle

For example, take a circle with length  $L = \pi/a$ . The continuous spectrum has exactly one spine, extending along the imaginary axis, with a simple point at each end, and a countable number of real double points:



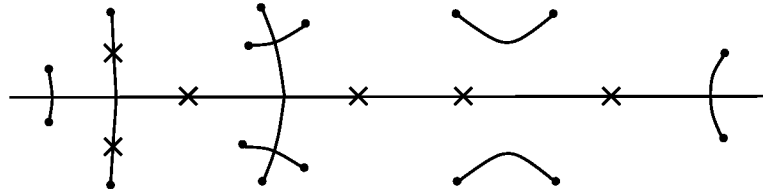
If we take the circle as multiply-covered, i.e.,  $L = m(\pi/a)$ , then continuous spectrum is the same, but double points (marked by X's here) proliferate along the real axis and along the spine:



In general, the Floquet spectrum is more complicated than this!

### 3.2. Properties of the Floquet Spectrum

The spectrum is symmetric under complex conjugation, and is unchanged by time evolution under the NLS. It contains the whole real line, plus (typically) spines branching off the real line, and possibly some disconnected bands. The bands end in simple points of the periodic spectrum, and multiple points can occur along the real axis or the bands/spines. So, a typical spectrum might look like this:



Finite-gap potentials are those for which the spectrum has finitely many simple points. I will talk more about the construction of finite-gap solutions later, right now, to answer the question about closure conditions, we need to define one more object, the quasimomentum function.

### 3.3. Closure and the Spectrum

For most  $\lambda$  values, there will be two linearly independent eigenvectors for the transfer matrix. Using such vectors as initial conditions gives solutions to the linear system, called **Bloch eigenfunctions**, that are periodic up to a multiplicative factor. Those factors are known as **Floquet multipliers**, and the **quasimomentum**  $p(\lambda)$  is  $-i$  times the logarithm of a Floquet multiplier. Because there are, in general, two Floquet multipliers for each  $\lambda$ , the quasimomentum is defined on a Riemann surface  $\Sigma$  that double-covers the complex  $\lambda$ -plane. (The covering is branched at the simple points.) Because  $e^{ip(\lambda)}$  and its reciprocal are eigenvalues of the transfer matrix, then  $\Delta(\lambda) = 2 \cos(p(\lambda))$ .

**Theorem (Grinevich and Schmidt [4]).**  $\gamma$  is smoothly closed at length  $L$  if and only if  $\Lambda_0$  is a real double point that is a zero of the quasimomentum differential  $dp$ , i.e.,

$$\Delta(\Lambda_0) = \pm 2, \quad \left. \frac{dp}{d\lambda} \right|_{\lambda=\Lambda_0} = 0, \quad \Lambda_0 \in \mathbb{R}.$$

One typically achieves this by picking  $\Lambda_0$  to be a double point that is also at the base of a spine, i.e. where a spine of the continuous spectrum intersects the real axis.

### 4. Constructing Finite-Gap Solutions

For a finite-gap potential, the Riemann surface  $\Sigma$  has finite genus. Conversely, we can begin with a finite collection of pairs of complex conjugate branch points and construct a finite-gap solution of NLS. The data necessary for this construction are a hyperelliptic curve  $\Sigma$  of genus  $g$ , with complex-conjugate branch points, and a nonspecial divisor  $\mathcal{D}$  on  $\Sigma$  that satisfies a certain reality condition (see [2] or [3] for details). The branch points will become the simple points for the spectrum of the resulting NLS solution, which has the form

$$q(x, t) = \exp(-iEx + iNt) \frac{\theta(i\mathbf{V}x + i\mathbf{W}t - \mathbf{D} + \mathbf{r})}{\theta(i\mathbf{V}x + i\mathbf{W}t - \mathbf{D})}.$$

Here, scalars  $E, N \in \mathbb{R}$  and vectors  $\mathbf{V}, \mathbf{W} \in \mathbb{R}^g$  and  $\mathbf{r} \in \mathbb{C}^g$  are determined by the periods of certain Abelian differentials on  $\Sigma$ , and the purely imaginary vector  $\mathbf{D} \in \mathbb{C}^g$  is computed using the divisor.

Formulas for finite-gap NLS solutions were first obtained by Its and Kotlyarov. Later, these solutions were re-interpreted by Krichever in terms of Baker–Akheizer functions on a complex curve (see [2] for references). There are also formulas for the Bloch eigenfunctions, and substituting these into the Sym formula yields formulas for components of the curve  $\gamma$  in  $\mathbb{R}^3$  (again, see [3] for details).



Figure 1.1: The figure-eight curve

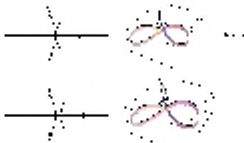


Figure 1.1 shows the figure-eight curve, which is a curve in  $\mathbb{R}^3$  that is the union of two curves. The figure-eight curve is a surface with a self-intersection. The curves are colored with a gradient from purple to red.

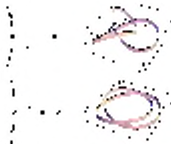
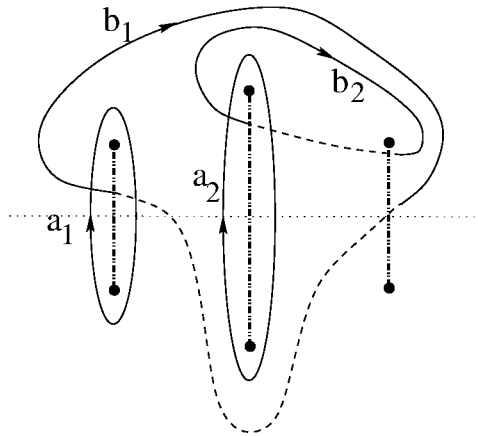


Figure 1.2 shows the figure-eight curve, which is a curve in  $\mathbb{R}^3$  that is the union of two curves. The figure-eight curve is a surface with a self-intersection. The curves are colored with a gradient from purple to red.

## 6. Symmetric Spectra

Here, we suppose the branch points of  $\Sigma$  are symmetric about the origin of the complex plane, as shown here for genus two.



(The diagram shows the branch points, along with branch cuts and a typical homology basis.)

Using the extra symmetry, we obtain the following

**Theorem** ([3]). *If  $g = 2$  or  $3$ , and  $\gamma(x, t)$  is constructed at  $\Lambda_0 = 0$ , then  $\gamma$  is **periodically planar**, i.e. planar at regular intervals in time.*

Moreover, the curves at different planar times are congruent, giving **breather solutions** for the filament flow. (For curves constructed using the Sym–Pöhlmeier formula at  $\Lambda_0 \neq 0$ , “constant torsion” replaces “planar” in the theorem.)

The above theorem is a corollary of a result that works in any genus, but involves an extra condition on the divisor which is vacuous in low genus. (So, higher-genus solutions may be periodically planar, but it depends on the divisor.) The proof is basically a calculation showing that, at certain times, the potential is a constant multiple of its complex conjugate. The calculation uses special algebraic properties of the ingredients for finite-gap solutions that arise when the Riemann surface has an extra automorphism induced by the symmetry (see [3] for details).

**Theorem** ([3]). *If  $g = 2$  the curve has a fixed plane of reflection symmetry.*

This typically means that the filament will have persistent self-intersections as it evolves. We also have observed experimentally that, between the planar times, these genus two solutions lie on spheres.

The following examples illustrate the phenomena described in the above theorems.





FIG. 1. Knot evolution.

Figure 1 shows the evolution of a knot in the presence of the topological interaction. The knot is initially a simple loop, but as the topological interaction is introduced, it becomes more complex. The knot is shown in three stages of evolution, with the topological interaction being introduced in the second stage.

The knot is shown in three stages of evolution. In the first stage, the knot is a simple loop. In the second stage, the knot is twisted and the topological interaction is introduced. In the third stage, the knot is further twisted and the topological interaction is shifted, resulting in a more complex knot structure.

The knot is shown in three stages of evolution. In the first stage, the knot is a simple loop. In the second stage, the knot is twisted and the topological interaction is introduced. In the third stage, the knot is further twisted and the topological interaction is shifted, resulting in a more complex knot structure.

$$\frac{dN}{dt} = \gamma \frac{N}{V}$$

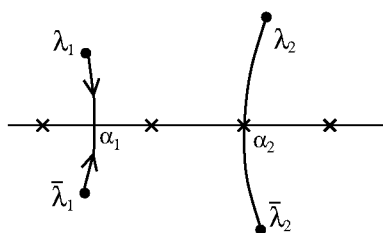
$$\frac{dN}{dt} = \gamma \frac{N}{V}$$

The knot is shown in three stages of evolution. In the first stage, the knot is a simple loop. In the second stage, the knot is twisted and the topological interaction is introduced. In the third stage, the knot is further twisted and the topological interaction is shifted, resulting in a more complex knot structure.

A couple of years ago, we realized that we could rig these isoperiodic deformations so that, if you start with one of the  $\alpha$ 's being a double point (i.e., the quasimomentum is  $\pm 1$  there), then it remains a double point, provided that the corresponding control is set to zero. Next, I will describe how this works in the elastic rod homotopy.

### 7.1. Collapse onto the Unit Circle

Suppose the genus is one, and  $\Lambda_0 = \alpha_2$  gives a closed curve. Then setting control  $c_2 = 0$  allows us to deform the spectrum while keeping the curve in  $\mathbb{R}^3$  closed. Since there is only one control function, we can reparametrize so that it is a constant. If we choose  $c_1 = -1$ , we hit a singularity in finite deformation time, when the pair  $(\lambda_1, \bar{\lambda}_1)$  collides with  $\alpha_1$  on the real axis.



We can reverse this process if we take  $c_1 = 1$ , and expand the trajectory coming out of the real double point as a power series in parameter  $u = \sqrt{\xi}$ .

This idea can be applied to arbitrary genus spectra that are “close” to that of a multiply-covered circle. If each complex conjugate pair of branch points is collapsed onto the real axis via isoperiodic deformations, then the components of the frequency vector before deformation can be calculated in terms of the residues of the limiting differentials, giving  $V_k = \pm 2 \lim \sqrt{1 + \alpha_k^2}$ , where  $\alpha_k$  limits onto a double point belonging to the periodic spectrum of a multiply-covered circle, and the sign of  $V_k$  is the same as the sign of  $\lim \alpha_k$ .

By reversing this collapse, we can construct a finite-gap solution with specified values for the frequencies, by successively opening up the appropriate double points for the multiply-covered circle. Namely, opening up the double point  $\alpha_k = \pm \sqrt{(m/n)^2 - 1}$ , which is in the spectrum for the  $n$ -times covered circle, gives  $V_k = \pm 2m/n$ .

### 7.2. Deforming the Circle to a Cable Knot

We have observed experimentally that, beginning with a multiply-covered circle and repeatedly opening up a real double point (using a closure-preserving, isoperiodic deformation) to a pair of new branch points a small distance away from the

Let  $\mathcal{C}$  be the complex plane with the origin removed and let  $\mathcal{C}^*$  be the universal covering space of  $\mathcal{C}$ . Let  $\mathcal{C}^*$  be the universal covering space of  $\mathcal{C}$ .

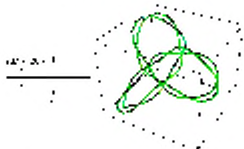
Let  $\mathcal{C}^*$  be the universal covering space of  $\mathcal{C}$ . Let  $\mathcal{C}^*$  be the universal covering space of  $\mathcal{C}$ .

Let  $\mathcal{C}^*$  be the universal covering space of  $\mathcal{C}$ . Let  $\mathcal{C}^*$  be the universal covering space of  $\mathcal{C}$ .



Let  $\mathcal{C}^*$  be the universal covering space of  $\mathcal{C}$ . Let  $\mathcal{C}^*$  be the universal covering space of  $\mathcal{C}$ .

Let  $\mathcal{C}^*$  be the universal covering space of  $\mathcal{C}$ . Let  $\mathcal{C}^*$  be the universal covering space of  $\mathcal{C}$ .



Let  $\mathbf{v}$  be a vector

field in the plane. In some cases, the vector field may be tangent to the boundary of the domain. In this case, the vector field is said to be tangent to the boundary.

Problem

1. Let  $\mathbf{v}$  be a vector field in the plane. In some cases, the vector field may be tangent to the boundary of the domain. In this case, the vector field is said to be tangent to the boundary.
2. Let  $\mathbf{v}$  be a vector field in the plane. In some cases, the vector field may be tangent to the boundary of the domain. In this case, the vector field is said to be tangent to the boundary.
3. Let  $\mathbf{v}$  be a vector field in the plane. In some cases, the vector field may be tangent to the boundary of the domain. In this case, the vector field is said to be tangent to the boundary.
4. Let  $\mathbf{v}$  be a vector field in the plane. In some cases, the vector field may be tangent to the boundary of the domain. In this case, the vector field is said to be tangent to the boundary.
5. Let  $\mathbf{v}$  be a vector field in the plane. In some cases, the vector field may be tangent to the boundary of the domain. In this case, the vector field is said to be tangent to the boundary.
6. Let  $\mathbf{v}$  be a vector field in the plane. In some cases, the vector field may be tangent to the boundary of the domain. In this case, the vector field is said to be tangent to the boundary.
7. Let  $\mathbf{v}$  be a vector field in the plane. In some cases, the vector field may be tangent to the boundary of the domain. In this case, the vector field is said to be tangent to the boundary.
8. Let  $\mathbf{v}$  be a vector field in the plane. In some cases, the vector field may be tangent to the boundary of the domain. In this case, the vector field is said to be tangent to the boundary.
9. Let  $\mathbf{v}$  be a vector field in the plane. In some cases, the vector field may be tangent to the boundary of the domain. In this case, the vector field is said to be tangent to the boundary.
10. Let  $\mathbf{v}$  be a vector field in the plane. In some cases, the vector field may be tangent to the boundary of the domain. In this case, the vector field is said to be tangent to the boundary.

- [8] Kida S., *A Vortex Filament Moving Without Change of Form*, J. Fluid Mech. **112** (1981) 397–409.
- [9] Langer J. and Perline R., *Poisson Geometry of the Filament Equation*, J. Nonlinear Sci. **1** (1991) 71–93.
- [10] Langer J. and Singer D., *Lagrangian Aspects of the Kirchhoff Elastic Rod*, SIAM Review **38** (1996) 605–618.